

Optimal focusing conditions for bright SPDC sources

Lorenzo Coccia,^{1,*} Alberto Santamato,^{2,3} Giuseppe Vallone,^{1,4} and Paolo Villoresi^{1,5,6}

¹*Dipartimento di Ingegneria dell'Informazione, Università degli Studi di Padova, via Gradenigo 6B, 35131 Padova, Italy*

²*CNIT, Via Moruzzi 1, Area di ricerca CNR, 56124 Pisa, Italy*

³*Nu Quantum Ltd., Broers Building, 21 JJ Thomson Avenue, Cambridge, CB3 0FA, United Kingdom*

⁴*Dipartimento di Fisica e Astronomia, Università degli Studi di Padova, via Marzolo 8, 35131 Padova, Italy*

⁵*Padua Quantum Technologies Research Center, Università degli Studi di Padova, via Gradenigo 6B, Padova, Italy*

⁶*Istituto di Fotonica e Nanotecnologie-CNR, via Trasea 7, 35131 Padova, Italy*

Optimizing the brightness of a spontaneous parametric down conversion (SPDC) source is an important task for many quantum information applications. We investigate the optimal focusing conditions to maximize the number of photons produced in an SPDC process and coupled with single mode fibers. We provide a general expression for the two-photon wavefunction, generalizing previous known results, by considering collinear and non-collinear emission. We present analytical expressions for our results in the thin crystal limit and clarify the relation between different focusing conditions already existing in the literature. Differently to what previously reported, we show that the optimal ratio between the pump waist and the generated photons waist depends on the emission angle: it is $1/\sqrt{2}$ for collinear degenerate emission and approaches $1/2$ for larger collection angles. The role of spectral filters is also analyzed. We support and enrich our discussion with numerical simulations, performed for Type I SPDC in a BBO crystal. For this type of emission, we also investigate the role of the transverse walk-off outside the thin crystal regime.

I. INTRODUCTION

Spontaneous parametric down conversion (SPDC) is one of the most commonly exploited physical mechanism to generate quantum states of light and it has been used for fundamental tests of quantum mechanics, as well as for the realization of many protocols of quantum cryptography [1, 2], teleportation [3] and optical computing [4, 5]. The production of photons in this process is typically realised by the interaction of a laser pump with a non-linear optical medium that must have a rather strong second-order non-linear optical susceptibility χ^2 in order to realize a bright source. However, many other factors determine quantity and properties of the emitted photons, such as phase matching and energy conservation relations, medium length and shape of the pump laser beam. The importance of these and others elements has been considered in many works with different types and degrees of approximation and we will not attempt to refer to them exhaustively. Instead, we are interested in a common experimental setup in which the photons involved in the SPDC process are emitted and collected by single-mode fibres (SMFs). Mathematically, this configuration can be schematized by assuming spatial Gaussian modes for the photons, as has been done in several papers [6–17]. In these works, different spectral properties of the emitted photons have been studied, using various perspectives or by invoking suitable approximations, such as the thin crystal limit.

In our paper, we will focus on the brightness of the

emission process, evaluated as

$$R_{\text{tot}} = \int |\Psi(\omega_i, \omega_s)|^2 d\omega_i d\omega_s, \quad (1)$$

where $\Psi(\omega_i, \omega_s)$ is the wavefunction describing the frequency spectrum of the two photons produced (denoted signal (s) and idler (i) as is customary), when they are coupled into single mode fibers.

It is well known that the brightness (1) depends on the waists of the photons in the process. According to the different assumptions carried on, however, different optimal values for the ratio between the pump waist and the signal/idler waists have been reported (see e.g. [8, 9]). To the best of our knowledge, a clear relation between the different optimal values proposed is missing.

Our article is part of this discussion, aiming to understand the conditions that lead to the optimal brightness in different regimes. Assuming Gaussian beams, we will tackle the problem from the momentum space perspective. We will first discuss how to make a known “paraxial” approximation [8] more accurate, providing an explicit formula, given in equation (26), to perform numerical simulations of the bi-photon wavefunction. Then, we will clarify the relation between values of optimal ratio already found in the literature, relating them to different experimental situations: collinear or non-collinear emission, with or without spectral filters. Moreover, we will study the role of the transverse walk-off and find new interesting optimal conditions.

To investigate different regimes and different geometrical configurations, we will adopt numerical computations, choosing standard BBO crystals to realize Type I emission. A privileged role will be played by the SPDC sources based on crystals which are *thin* with respect to the focal depth of the pump field inside the crystal itself. In this particular configuration, we will derive analytical

* lorenzo.coccia@unipd.it

expressions to better understand the numerical results

The paper is organized as follows. In the next section we introduce the assumptions of our work. In Section III we describe the paraxial approximation and derive formulas for the bi-photon wavefunction. In Section IV we discuss the thin crystal limit and clarify the relation between the optimal focusing conditions proposed in the literature. In Section V we study corrections to the thin limit and report our numerical simulations, before concluding in Section VI. Some technical details are gathered in three appendices.

II. DEFINITIONS AND ASSUMPTIONS

The interaction Hamiltonian describing an SPDC process can be written as

$$\hat{\mathcal{H}}_I = \zeta_{\text{eff}}^{(2)} \int_V d^3\mathbf{r} \hat{D}_p^{(+)} \hat{D}_s^{(-)} \hat{D}_i^{(-)} \quad (2)$$

with $\zeta_{\text{eff}}^{(2)}$ the inverse effective susceptibility characterizing the interaction and V the volume of the non-linear medium, which for us will be an uniaxial crystal. \hat{D}_a , with $a = p, s, i$, are the displacement field operators of pump (p), signal (s) and idler (i) and their apexes denote if we are considering annihilation (+) or creation (-) operators. Note that we are writing the Hamiltonian in terms of \hat{D}_a and not of the electric fields, since the latter choice would lead some contradictions in the quantization procedure, as discussed in [18]. See also [19] for a review. In our discussion we will be rather general without choosing a particular polarization for the photons. If not otherwise stated, we will restrict to a specific type of SPDC (Type I) only for numerical simulations.

We consider a pulsed laser which propagates along the z -direction, impinging on a crystal of length L , centered at $z = 0$ and oriented perpendicular to z -axis. We choose the y -axis so that the optical axis lies on the (y, z) plane, while the x -axis is defined by the left hand rule. Following [8, 20], we parameterize the beam by using the frequency $\omega_p = 2\pi n_p c / \lambda_p$ and the wavevector components $\mathbf{k}_p = (k_{px}, k_{py})$ perpendicular to the propagation direction, which are quantities preserved at the crystal-free space interface. As customary, we consider a strong pump field so that we can ignore depletion and we can write it as a classical field

$$D_p^{(+)}(\mathbf{r}, t) = \frac{\mathcal{D}_p}{(2\pi)^{\frac{3}{2}}} \int d^2\mathbf{k}_p d\omega_p \mathcal{A}_p(\omega_p, \mathbf{k}_p) e^{-i(\mathbf{k}_p, k_{pz}) \cdot \mathbf{r}} e^{-i\omega_p t} \quad (3)$$

Here, $\mathbf{r} = (x, y, z)$ and \mathcal{D}_p parameterizes the amplitude of the field. We also assumed the factorable form

$$\mathcal{A}_p(\omega_p, \mathbf{k}_p) = \mathcal{A}_p^{\text{temp}}(\omega_p) u_p(\mathbf{k}_p) \quad (4)$$

with a temporal normalized wavefunction given by $\mathcal{A}_p^{\text{temp}}(\omega_p)$ and a spatial normalized wavefunction given by $u_p(\mathbf{k}_p)$. The same parameterization, based on the frequency and the x, y wavevector components, will be used

for the signal and idler photons produced in the SPDC process. For the signal we have

$$\hat{D}_s^{(-)}(\mathbf{r}, t) = \frac{\mathcal{D}_s}{(2\pi)^{\frac{3}{2}}} \int d^2\mathbf{k}_s d\omega_s e^{i(\mathbf{k}_s, k_{sz}) \cdot \mathbf{r}} e^{i\omega_s t} \hat{a}^\dagger(\mathbf{k}_s, \omega_s) \quad (5)$$

and similarly for the idler, replacing s with i .

Keeping only the first order expansion of the evolution operator, the bi-photon wavefunction, describing the photons emitted in the process, is given by

$$|\Psi\rangle = -\frac{i}{\hbar} \int_{-\infty}^{\infty} dt \hat{\mathcal{H}}_I(t) |\text{initial}\rangle \quad (6)$$

Assuming that the photons are created in spatial modes described by $u_s(\mathbf{k}_s, \omega_s)$ and $u_i(\mathbf{k}_i, \omega_i)$, we can easily find the following expression (see also [8])

$$\Psi(\omega_i, \omega_s) = \mathcal{N} \mathcal{A}_p^{\text{temp}}(\omega_i + \omega_s) \Phi(\omega_i, \omega_s) \quad (7)$$

where, rescaling the z coordinate as $z = LZ/2$,

$$\begin{aligned} \Phi(\omega_i, \omega_s) = & \frac{L}{2} \int d^2\mathbf{k}_i d^2\mathbf{k}_s \int_{-1}^1 dZ u_p(\mathbf{k}_i + \mathbf{k}_s) \times \\ & \times u_s^*(\mathbf{k}_s, \omega_s) u_i^*(\mathbf{k}_i, \omega_i) e^{-i\frac{L}{2} Z \Delta k_z(\mathbf{k}_i, \omega_i; \mathbf{k}_s, \omega_s)}. \end{aligned} \quad (8)$$

To derive this formula, we integrated over the time and the transverse spatial coordinates, obtaining the conditions $\omega_p = \omega_i + \omega_s$ and $\mathbf{k}_p = \mathbf{k}_i + \mathbf{k}_s$ in the form of delta functions. Note that we also consider the possibility of spatial poling, so that the normalization constant \mathcal{N} in (7) is written in terms of the amplitudes of the displacement fields as $\mathcal{N} = \zeta_{\text{eff}}^{(2)} \mathcal{D}_p \mathcal{D}_i \mathcal{D}_s G_m / i\hbar$, with G_m Fourier coefficient of the spatial poling distribution of order m [21]. Calling Λ the spatial poling period, at order m the phase mismatch Δk_z is

$$\begin{aligned} \Delta k_z(\mathbf{k}_i, \omega_i; \mathbf{k}_s, \omega_s) = & m \frac{2\pi}{\Lambda} + k_{pz}(\mathbf{k}_i + \mathbf{k}_s, \omega_i + \omega_s) + \\ & - k_{iz}(\mathbf{k}_i, \omega_i) - k_{sz}(\mathbf{k}_s, \omega_s), \end{aligned} \quad (9)$$

where k_{az} are the longitudinal components of the wavevectors inside the crystal. Unpoled crystals correspond to $m = 0$.

For uniaxial crystals, the explicit form of $k_{az}(\mathbf{k}_a, \omega_a)$ depends on the polarization of the corresponding wave. Writing the ordinary and the extraordinary refraction indices as n_o and n_e , the refraction index at an angle θ to the optical axis is

$$\frac{1}{n_\theta^2} = \frac{\sin^2 \theta}{n_e^2} + \frac{\cos^2 \theta}{n_o^2}. \quad (10)$$

We can write

$$k_z(\mathbf{k}, \omega) = \beta k_y + \sqrt{\left(\frac{n\omega}{c}\right)^2 - (\gamma k_x)^2 - \left(\gamma \frac{n}{n_o} k_y\right)^2} \quad (11)$$

where $\beta = (\gamma^2 - \frac{n_o^2}{n_e^2}) \sin \theta \cos \theta$ and the values of the parameters depends on the polarization as follows

$$\text{extraordinary : } n = n_\theta, \quad \gamma = \frac{n_\theta}{n_e}, \quad (12)$$

$$\text{ordinary : } n = n_o, \quad \gamma = 1. \quad (13)$$

More details can be found in Appendix A. Note that the dependence on ω is also implicit in the indexes of refraction $n_o(\omega)$ and $n_e(\omega)$ and thus in $\beta(\omega)$, $n(\omega)$ and $\gamma(\omega)$. According to the type of phase-matching considered, it is necessary to express the longitudinal component of the wavevectors k_{az} by using equations (11) and (12) or (13).

The above derived two-photons wavefunction (7) is very general. We will now focus on some experimentally relevant cases, as done in [8]. First, we will assume the spectral pump function to be a normalized Gaussian, namely

$$\mathcal{A}_p^{\text{temp}}(\omega_p) = \sqrt[4]{\frac{2\tau_p^2}{\pi}} e^{-\tau_p^2(\omega_p - \omega_0)^2} \quad (14)$$

with τ_p the pulse duration. Then, in the experimental setup we have in mind, the photons are emitted and collected using single mode fibers. We can therefore try to approximate their spatial wavefunctions using Gaussians

$$u_a(\mathbf{k}_a, \omega_a) = \sqrt{\frac{w_{ax}w_{ay}}{2\pi}} \prod_{\mu=x,y} e^{-\frac{w_{a\mu}^2}{4}(k_{a\mu} - k_{0a\mu})^2}, \quad (15)$$

where $a = p, i, s$, $k_{0p\mu} = 0$ and $k_{0s\mu}, k_{0i\mu}$ are the central wavevectors corresponding to the directions where the photons are collected. The parameters $w_{a\mu}$ are the *beam waists*: we consider the possibility that the beams are elliptic, meaning that the beam waists w_{ax} and w_{ay} can be different.

Finally, we choose \mathbf{k}_{0i} and \mathbf{k}_{0s} such that the phase matching (PM) and energy matching (EM) conditions are satisfied for the idler and signal photons at frequencies Ω_i and Ω_s , namely

$$\begin{cases} \Delta k_z(\mathbf{k}_{0i}, \Omega_i; \mathbf{k}_{0s}, \Omega_s) = 0 & \text{phase matching } \parallel, \\ \mathbf{k}_{0i}(\Omega_i) + \mathbf{k}_{0s}(\Omega_s) = 0 & \text{phase matching } \perp, \\ \Omega_i + \Omega_s = \omega_0 & \text{energy matching.} \end{cases} \quad (16)$$

Considering the phase matching condition, the central wavevectors can be written as

$$\mathbf{k}_{0i} = \frac{\omega_i \sin \alpha_i}{c} \mathbf{u}, \quad \mathbf{k}_{0s} = -\frac{\omega_s \sin \alpha_s}{c} \mathbf{u}, \quad (17)$$

where \mathbf{u} is a versor in the (x, y) plane and α_i, α_s are the angles of collection direction that are related by $\Omega_i \sin \alpha_i = \Omega_s \sin \alpha_s$ to satisfy the transverse (\perp) phase matching condition of (16). The description (15) holds for small angles of collection (see Appendix B) so that in (17) we will approximate the sine function with its argument.

III. PARAXIAL APPROXIMATION

The actual computation of the integrals in (8) is rather difficult, due to the complicated dependence of Δk_z on the transverse components, as clear from (11). However, we can note that the absolute value of the integrand in (8) is given by the product of the spatial wavefunctions u_a , i.e., up to an overall factor,

$$\prod_{\mu=x,y} e^{-\frac{w_{i\mu}^2}{4}(k_{i\mu} - k_{0i\mu})^2 - \frac{w_{s\mu}^2}{4}(k_{s\mu} - k_{0s\mu})^2 - \frac{w_{p\mu}^2}{4}k_{p\mu}^2} \quad (18)$$

with $k_{p\mu} = k_{i\mu} + k_{s\mu}$. This quantity is strongly peaked around its maximum if

$$w_{a\mu} \gg \lambda_a, \quad a = i, s, p \quad (19)$$

a condition that is satisfied in typical SPDC sources. We can then apply the so called paraxial approximation: a small error can be made in the computation of (8) by expanding Δk_z at the second order around the maximum of (18) which occurs, for each component $\mu = x, y$, at

$$\begin{aligned} \bar{k}_{i\mu}(\omega_i, \omega_s) &= k_{0i\mu}(\omega_i) - \frac{\bar{w}_{i\mu}^2}{w_{i\mu}^2} [k_{0i\mu}(\omega_i) + k_{0s\mu}(\omega_s)] \\ \bar{k}_{s\mu}(\omega_i, \omega_s) &= k_{0s\mu}(\omega_s) - \frac{\bar{w}_{s\mu}^2}{w_{s\mu}^2} [k_{0i\mu}(\omega_i) + k_{0s\mu}(\omega_s)] \end{aligned} \quad (20)$$

where we introduced the *effective* beam waist \bar{w}_μ :

$$\frac{1}{\bar{w}_\mu^2} = \frac{1}{w_{p\mu}^2} + \frac{1}{w_{i\mu}^2} + \frac{1}{w_{s\mu}^2}. \quad (21)$$

Note that, although similar in spirit, our approximation around the vectors $\bar{\mathbf{k}}_i$ and $\bar{\mathbf{k}}_s$ is different from the one discussed in [8], where the expansion is simply performed around the center of the two Gaussians \mathbf{k}_{0i} and \mathbf{k}_{0s} . Since $\bar{k}_{i\mu}(\Omega_i, \Omega_s) = k_{0i\mu}(\Omega_i)$ and $\bar{k}_{s\mu}(\Omega_i, \Omega_s) = k_{0s\mu}(\Omega_s)$, the two approximations are equivalent for the central frequencies Ω_i and Ω_s , but the expansion around \mathbf{k}_{0i} and \mathbf{k}_{0s} is not centered on the maximum of the exponential for other values of ω_i and ω_s . Therefore, our choice gives a more accurate approximation of $\Phi(\omega_i, \omega_s)$ with respect to the one performed in [8] when $\omega_i \neq \Omega_i$ and $\omega_s \neq \Omega_s$. An example is given in Figure 1.

To expand Δk_z to second order, we first expand each longitudinal component k_{az} as

$$k_{az} \approx \bar{k}_{az} + \sum_{\mu} (k_{\mu} - \bar{k}_{\mu}) K_{1a}^{\mu} + \frac{1}{2} \sum_{\mu\nu} (k_{\mu} - \bar{k}_{\mu})(k_{\nu} - \bar{k}_{\nu}) K_{2a}^{\mu\nu} \quad (22)$$

where $\bar{k}_{az} = k_{az}(\bar{\mathbf{k}}_a)$, $\bar{\mathbf{k}}_a = (\bar{k}_{ax}, \bar{k}_{ay})$ and we introduced the derivatives

$$K_{1a}^{\mu} = \left. \frac{\partial k_{az}}{\partial k_{a\mu}} \right|_{\mathbf{k}_a = \bar{\mathbf{k}}_a}, \quad K_{2a}^{\mu\nu} = \left. \frac{\partial^2 k_{az}}{\partial k_{a\mu} \partial k_{a\nu}} \right|_{\mathbf{k}_a = \bar{\mathbf{k}}_a}. \quad (23)$$

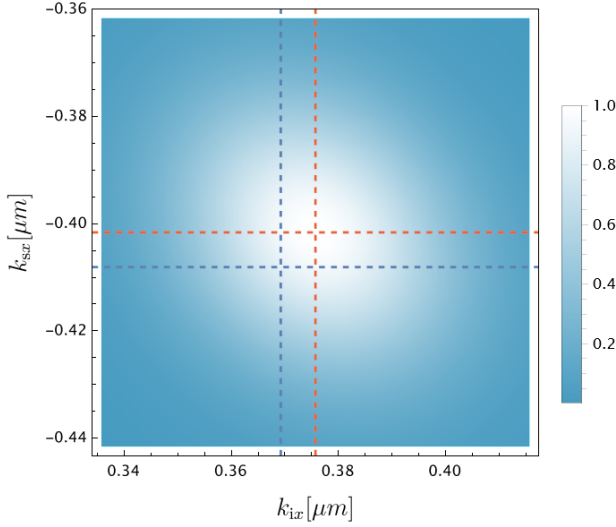


Figure 1. Normalized absolute value of the integrand in (8) as function of k_{ix} and k_{sx} , for $\omega_i = \omega_0/2.1$ and $\omega_s = \omega_0/1.9$. The red dotted lines denote the values of \bar{k}_{ax} and the blue ones the values of k_{a0x} . The simulation has been performed for a Type I SPDC realized via a BBO crystal with $\lambda_0 = 2\pi c/\omega_0 = 405$ nm, perfect phase matching, collection angle $\alpha \approx 2.8^\circ$ in the (x, z) plane, $w_i = w_s = 50$ μm and $w_p = 25$ μm .

In the previous equation we also defined

$$\bar{k}_{p\mu}(\omega_i, \omega_s) = \bar{k}_{i\mu} + \bar{k}_{s\mu} = \left(\frac{\bar{w}_\mu}{w_{p\mu}} \right)^2 (k_{0i\mu} + k_{0s\mu}). \quad (24)$$

With the substitution (22), the resulting integral in (8) becomes Gaussian in the transverse components, and can be solved. The result can be expressed in terms of some physical relevant quantities. Indeed, we can introduce the *focal parameter* ($\xi_{a\mu}$) and the *deviation parameter* ($\nu_{a\mu}$), given by

$$\xi_{a\mu}(\omega_a) = -\frac{L}{w_{a\mu}^2} K_{2a}^{\mu\mu}, \quad \nu_{a\mu}(\omega_a) = -\frac{L}{2w_{a\mu}} K_{1a}^\mu. \quad (25)$$

As discussed in Appendix B, the parameter ν_μ is related to the lateral deviation of the beam (in units of beam waist w_μ inside the crystal) since, at the output of the crystal, the beam is shifted by $w_{a\mu}\nu_{a\mu}$. The parameter ξ_μ , instead, is related to the focusing condition of the beam in the μ direction [6]: if $\xi_\mu \gg 1$ ($\xi_\mu \ll 1$) the field is strongly (weakly) focused relative to the length L of the crystal.

Leaving to the Appendix C a more general expression of the bi-photon wavefunction, we here report the case in which the photons are collected in the (x, z) or the (y, z) plane, a very common choice in experiments. In this configuration, the expression (8) in the paraxial ap-

proximation becomes

$$\begin{aligned} \Psi(\omega_i, \omega_s) &= 2\sqrt{2\pi} L \mathcal{N} \mathcal{A}_p^{\text{temp}}(\omega_p) \times \\ &\times \prod_{\mu=x,y} \left(\frac{\bar{w}_\mu e^{-\frac{1}{4}\bar{w}_\mu^2(k_{0i\mu}+k_{0s\mu})^2}}{\sqrt{w_{p\mu} w_{i\mu} w_{s\mu}}} \right) \times \\ &\times \int_{-1}^1 dZ e^{-\frac{iL\Delta\bar{k}_z}{2} Z} \prod_{\mu=x,y} \frac{\exp(-Z^2 \frac{Q_\mu(Z)}{F_\mu(Z)})}{\sqrt{F_\mu(Z)}} \end{aligned} \quad (26)$$

where $\Delta\bar{k}_z = \Delta k_z(\bar{\mathbf{k}}_s, \omega_s; \bar{\mathbf{k}}_i, \omega_i)$ and

$$Q_\mu(Z) = A_\mu - iB_\mu Z, \quad (27)$$

$$F_\mu(Z) = 1 + i\xi_\mu Z + C_\mu Z^2. \quad (28)$$

Introducing the combination of waists and deviation parameters

$$\Delta_{ab\mu}^2 = \bar{w}_\mu^2 \left(\frac{\nu_{a\mu}}{w_{b\mu}} - \frac{\nu_{b\mu}}{w_{a\mu}} \right)^2, \quad (29)$$

the terms in Q_μ are given by

$$A_\mu = \Delta_{is\mu}^2 + \Delta_{ps\mu}^2 + \Delta_{pi\mu}^2, \quad (30)$$

$$B_\mu = \Delta_{is\mu}^2 \xi_{p\mu} - \Delta_{ps\mu}^2 \xi_{i\mu} - \Delta_{pi\mu}^2 \xi_{s\mu}. \quad (31)$$

The expression of $F_\mu(Z)$ in (28), instead, is written in terms of an aggregate focal parameter

$$\xi_\mu = \xi_{i\mu} \left(1 - \frac{\bar{w}_\mu^2}{w_{i\mu}^2} \right) + \xi_{s\mu} \left(1 - \frac{\bar{w}_\mu^2}{w_{s\mu}^2} \right) - \xi_{p\mu} \left(1 - \frac{\bar{w}_\mu^2}{w_{p\mu}^2} \right) \quad (32)$$

and the quantity

$$C_\mu = \bar{w}_\mu^2 \left(\frac{\xi_{s\mu} \xi_{p\mu}}{w_{i\mu}^2} + \frac{\xi_{i\mu} \xi_{p\mu}}{w_{s\mu}^2} - \frac{\xi_{i\mu} \xi_{s\mu}}{w_{p\mu}^2} \right) \quad (33)$$

which have been already introduced and discussed for the collinear SPDC in [6] (equations (14) and (15)).

Equation (26) is the first main result of this work: it is a generalization of the expression (16) of [6], taking into account more general angles of emission, birefringence effects and possible transverse walk-off the beams (see Appendix B for a discussion on this point). We note that, the result obtained in Equation (16) of [6] is recovered, up to different conventions in the overall factor, by noticing that in the case of periodically poled crystals with collinear emission we have $Q_\mu(Z) = 0$ and $\mathbf{k}_{0i} = \mathbf{k}_{0s} = 0$. Equation (26) is also an improvement and simplification with respect to the results contained in [8]. The differences are in the improved choice of expansion, as already discussed, and in the factorization of the integrand in the x, y components, due to the particular choice of the plane of emission.

IV. THIN CRYSTAL APPROXIMATION

For the rest of the work, we will be interested in studying the total brightness (1), starting from some analytical results that can be obtained in the limit of *thin crystals*. By this name we mean two conditions: first we require the length L of the crystal to be short with respect to the confocal parameter of the Gaussian beams corresponding to pump, idler and signal photons. Moreover, we ask the lateral deviation of the beams to be negligible with respect to the beam waists. Mathematically, these conditions can be expressed in terms of the parameters in (25) as

$$\xi_{a\mu} \ll 1, \quad \nu_{a\mu} \ll 1, \quad \forall a, \mu. \quad (34)$$

At order 0 in the expansion in $\nu_{a\mu}$ and $\xi_{a\mu}$, the Z -integral in (26) is simplified into

$$\begin{aligned} \Psi(\omega_i, \omega_s) &= 4\sqrt{2\pi}\mathcal{N}L\mathcal{A}_p^{\text{temp}}(\omega_i + \omega_s) \times \\ &\times \text{sinc}\left(\frac{L\Delta\bar{k}_z(\omega_i, \omega_s)}{2}\right) \times \\ &\times \prod_{\mu=x,y} \left(\frac{\bar{w}_\mu^2}{w_{p\mu}w_{i\mu}w_{s\mu}}\right)^{\frac{1}{2}} e^{-\frac{\bar{w}_\mu^2}{4}(k_{0i\mu} + k_{0s\mu})^2}. \end{aligned} \quad (35)$$

Actually, starting from the more general equations in (C8), it can be verified that the previous expression holds regardless of the choice of collection plane.

To focus on the main aspects of the problem, we can take symmetric waists in the x and y axes and

$$w_i = w_s = w, \quad w_p = rw \quad (36)$$

so that

$$\bar{w}^2 = \frac{r^2 w^2}{1 + 2r^2}. \quad (37)$$

This configuration is physically relevant since signal and idler are often collected in identical fibers, using symmetrical optical apparatuses. Moreover, we are interested in degenerate emission $\Omega_i = \Omega_s = \omega_0/2$ that implies, according to equation (16), equal angles of collection

$$\alpha_i = \alpha_s \equiv \alpha. \quad (38)$$

With this choice, by writing

$$\begin{aligned} \mathbf{k}_{0s} &= (k_{0sx}, k_{0sy}) = \frac{\omega_s \alpha}{c} (\cos \phi, \sin \phi), \\ \mathbf{k}_{0i} &= (k_{0ix}, k_{0iy}) = -\frac{\omega_i \alpha}{c} (\cos \phi, \sin \phi) \end{aligned} \quad (39)$$

we have

$$\sum_{\mu=x,y} \frac{\bar{w}^2}{4} (k_{0i\mu} + k_{0s\mu})^2 = \frac{\bar{w}^2 \alpha^2}{4c^2} (\omega_s - \omega_i)^2. \quad (40)$$

Nonetheless, the following discussion can be generalized to arbitrary parameters.

A. Longitudinal perfect phase matching

Our main goal is to find the optimal focusing conditions in order to have a bright source: in the configuration (36) this corresponds to finding the optimal values of w and r to maximize (1). To begin with, we can consider this problem when the longitudinal phase mismatch satisfies $L\Delta\bar{k}_z \ll 1$ for all the values of ω_i and ω_s that do not suppress the two Gaussian terms in (35). In this case, which we will call *longitudinal perfect phase matching*, the sinc term is ≈ 1 and the constraints to the spectral properties of Ψ are due to the coherence length τ_p of the pump, the central frequency ω_0 of the pump, the collection angle α and the beam waists. This condition is clearly more reasonable in presence of short crystals (L small) and when there is a good spatial overlap between the photons inside the crystal. Also, it is better satisfied in presence of spectral filters, but we will consider this configuration in Section IV B.

In this subsection, the only restriction to the collected frequencies is given by the finite transmission range of the crystal used in the SPDC process. In a first approximation, we can model the transmission range with a step-function: calling ω_b and ω_t the minimum and the maximal frequencies transmitted in a material, we impose the conditions

$$\omega_b \leq \omega_i, \omega_s, \omega_p \leq \omega_t \quad (41)$$

and we recall that $\omega_p = \omega_i + \omega_s$. These constraints restrict the integration domain in (1) and, in longitudinal perfect phase matching, we obtain

$$R_{\text{tot}} \propto \int_{\omega_b \leq \omega_i, \omega_s, \omega_i + \omega_s \leq \omega_t} d\omega_i d\omega_s e^{-2\tau_p^2(\omega_i + \omega_s - \omega_0)^2 - \frac{\bar{w}^2}{2c^2} \alpha^2 (\omega_i - \omega_s)^2}. \quad (42)$$

After performing the change of variables $u = \omega_i + \omega_s$, $v = \omega_i - \omega_s$ and solving the integral in v , we arrive at

$$\begin{aligned} R_{\text{tot}} &= 32\pi\mathcal{N}^2 L^2 \frac{\tau_p c \bar{w}^3}{\alpha r^2 w^6} \times \\ &\times \int_{2\omega_b}^{\omega_t} du e^{-2\tau_p^2(u - \omega_0)^2} \text{erf}\left(\frac{\bar{w}\alpha}{\sqrt{2}c}(u - 2\omega_b)\right) \end{aligned} \quad (43)$$

where erf denotes the error function and we restored the overall coefficients. We are interested in small angles α , so it is useful to define $x = u - 2\omega_b$ and consider the Maclaurin series

$$\text{erf}\left(\frac{\bar{w}\alpha}{\sqrt{2}c}x\right) = \frac{2}{\sqrt{\pi}} \sum_{n=0}^{\infty} \frac{(-1)^n}{n!(2n+1)} \left(\frac{\bar{w}\alpha}{\sqrt{2}c}x\right)^{2n+1}. \quad (44)$$

Plugging this expansion in (43) and inverting the order of sum and integral, we can write the total brightness as

$$\begin{aligned} R_{\text{tot}} &= 32L^2\mathcal{N}^2 \frac{r^2\sqrt{2\pi}}{(1+2r^2)^2 w^2 \tau_p} \times \\ &\times \sum_{n=0}^{\infty} \frac{(-1)^n}{2^n(1+2n)n!} \left(\frac{r^2}{1+2r^2}\right)^n \left(\frac{\alpha w}{\tau_p c}\right)^{2n} d_n \end{aligned} \quad (45)$$

where we introduced

$$d_n = \int_0^{\tau_p(\omega_t - 2\omega_b)} dy e^{-2(y + \tau_p(2\omega_b - \omega_0))^2} y^{1+2n}. \quad (46)$$

The integral defining d_n can be solved for each n , but its expression is not particularly useful for our discussion. Instead, we are more interested in understanding some limiting situations in which the series (44) (and consequently (45)) can be truncated or simplified. The relevant quantity is the argument of the erf in the central value ω_0 , namely the adimensional parameter $(\alpha w(\omega_0 - 2\omega_b)/c)$.

1. Collinear case

When $\alpha = 0$ or more generally the quantity $\alpha w(\omega_0 - 2\omega_b)$ is very small compared with c , the series (44) can be truncated at order 0. In this case, the brightness becomes

$$R_{\text{tot}} = 32L^2 \mathcal{N}^2 \frac{r^2 \sqrt{2\pi}}{(1 + 2r^2)^2 w^2 \tau_p} d_0. \quad (47)$$

The maximum of (47) is clearly at

$$r^* = \frac{1}{\sqrt{2}}. \quad (48)$$

This optimal condition emerges in the discussions of various previous works [6, 9, 17] studying collinear emission or assuming perfect transverse phase matching. Indeed, the latter condition corresponds to not having the second term in the exponential of (42), as is in the collinear case. Note that the brightness (47) increases by decreasing w but the divergence in $w = 0$ is not physical since we can't apply the thin crystal approximation for small values of w and, before that, we can't apply the paraxial approximation for waists of the same order of the wavelengths.

2. Large emission angle

Another interesting limit is the one in which $\alpha w(\omega_0 - 2\omega_b)$ is much larger than c . In this case the integral in (43) can be solved by replacing the erf function with its asymptotical value 1. Note that this substitution introduces an error of less than one per cent for arguments $x \gtrsim 2\sqrt{2}c/(\bar{w}\alpha)$. The resulting brightness is

$$R_{\text{tot}} = 8\sqrt{2}L^2 \mathcal{N}^2 c \frac{\pi^{3/2} r}{(1 + 2r^2)^{3/2} w^3 \alpha} \times \left(\text{erf}\left(\sqrt{2}\tau_p(\omega_0 - 2\omega_b)\right) - \text{erf}\left(\sqrt{2}\tau_p(\omega_0 - \omega_t)\right) \right) \quad (49)$$

with maximum at

$$r^* = \frac{1}{2}. \quad (50)$$

The expression (49) was also derived in [8], for the case of large $\tau_p \omega_0$ and integrating over the whole plane of the frequencies (ω_i, ω_s) . In fact, the integral in (42) is made of two exponential terms which select, in the plane of integration (ω_i, ω_s) , a contribution from a strip around the line $\omega_s = -\omega_i + \omega_0$ and another around the line $\omega_i = \omega_s$. The ‘‘width’’ of the strips depends on the value of τ_p and αw respectively. The intersection of the two strips gives the domain which is relevant for the integration. As αw and τ_p increase, this domain becomes smaller and smaller and we can expand the extrema of integration in the integral (42) to $(-\infty, \infty)$, as discussed in [7]. In this way, the integration can be performed via standard techniques recovering the result of [8]. We stress, however, that (49) only holds when $\alpha w(\omega_0 - 2\omega_b) \gg c$. For this reason, the divergence at $\alpha w = 0$ in (49) is unphysical.

a. Optimal angle in the (x, y) plane In case of sufficiently large emission angles, we can ask whether the rate emission is constant in the plane (x, y) . For equal waists $w_{ax} = w_{ay}$, we just found that there is no dependence on the direction in the (x, y) plane. However, we can try to generalize the previous result as follows. Let us relax, only in this paragraph, the conditions (36) and assume different waists on the x and y directions and between idler and signal. Integrating the frequencies over the whole real axes, the brightness is

$$R_{\text{tot}} \propto \frac{1}{\sqrt{\bar{w}_x^2 \cos^2 \phi + \bar{w}_y^2 \sin^2 \phi}} \prod_{\mu=x,y} \frac{\bar{w}_\mu^2}{w_{p\mu} w_{i\mu} w_{s\mu}}, \quad (51)$$

where we used the definitions in (39). Assuming fixed the waists $w_{p\mu}$, $w_{i\mu}$ and $w_{s\mu}$, we can find the best emission angle by minimizing the square root in (51), which gives ($n \in \mathbb{Z}$)

$$\begin{cases} \phi = (2n + 1)\frac{\pi}{2}, & \text{if } \bar{w}_x > \bar{w}_y \\ \phi = n\pi, & \text{if } \bar{w}_x < \bar{w}_y \end{cases} \quad (52)$$

while, if $\bar{w}_x = \bar{w}_y$ there isn't a privileged angle of emission, as found before. Therefore, the optimal emission plane is related to the direction of maximal value of the effective beam waist.

3. Intermediate values

For intermediate values of $\alpha w(\omega_0 - 2\omega_b)$, it is natural to expect a smooth transition between the values $r^* = 1/\sqrt{2}$ and $r^* = 1/2$. We checked this behaviour numerically by maximizing the expression in (43). The results are shown in Figure 2 where the simulations have been performed for three different values of the waist w , $\tau_p = 10^2$ fs and with a free space central pump wavelength $\lambda_0 = 405$ nm. The domain of integration has been chosen between the frequencies corresponding to $\lambda_b = 0.2$ nm and $\lambda_t = 2.2$ nm, i.e. in the clear transmission range of a BBO crystal, discussed in [22].

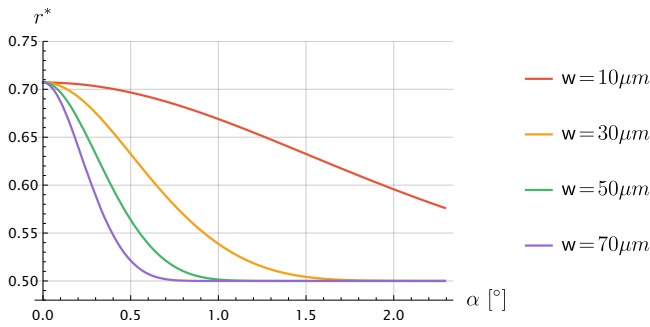


Figure 2. Value of the optimal r that maximize (43) in function of α . The optimal r changes in the region $r \in [\frac{1}{2}, \frac{1}{\sqrt{2}}]$.

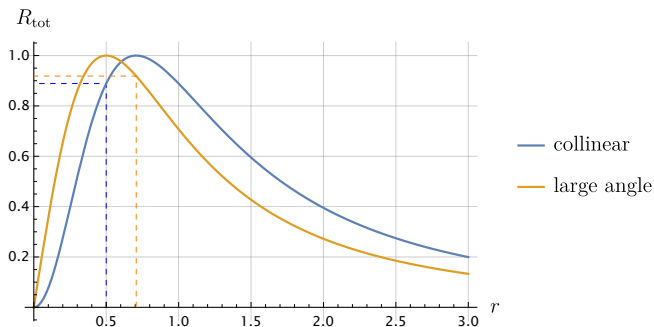


Figure 3. Variation of the (normalized) brightness as function of the ratio r , for collinear (47) and non-collinear (49) emission.

As a conclusion, we have shown how the waist ratio $r = w_p/w_s = w_p/w_i$ can be chosen to optimize the source brightness. The value $r^* = 1/\sqrt{2}$ is reported in the literature as the optimal value in the thin-crystal approximation and for collinear emission [9, 17], without reference to different values of the emission cone aperture. We have here demonstrated instead that the optimal r depends on the emission angle, as shown in Figure 2. For large aperture, we obtained $r^* = 1/2$, a value already derived in [8] without the crucial observation that it only holds in the limit of large emission aperture angle. Note that the right choice of the optimal ratio is quite relevant. As shown in Figure 3, by choosing $r = 1/2$ in the collinear case, instead of the optimal value $r = 1/\sqrt{2}$, there is a loss of brightness of around 10%. A similar situation holds in the non-collinear case, inverting the two values.

B. Spectral filters

In many experimental and technological implementations, only the photons in a small wavelength range are desired and spectral filters are inserted before collecting signal and idler. To reproduce this setup, we assume that the filters act as step functions and impose on the idler

and signal frequencies the restriction

$$\frac{\omega_0}{2} - \delta \leq \omega_i, \omega_s \leq \frac{\omega_0}{2} + \delta \quad (53)$$

where 2δ denotes the frequency width selected by the filters. The corresponding brightness is

$$R_{\text{tot}} = 32\pi\mathcal{N}^2 L^2 \frac{\tau_p c \bar{w}^3}{\alpha r^2 w^6} \int_{-2\delta}^{2\delta} du e^{-2\tau_p^2 u^2} \operatorname{erf}\left(\frac{\bar{w}\alpha}{\sqrt{2}c}(2\delta - |u|)\right) \quad (54)$$

where, starting from (43) with the constraints (53), we performed the change of variables $u = \omega_i + \omega_s - \omega_0$, $v = \omega_i - \omega_s$ and we solved the integral in v . For sufficiently narrow filters, $\delta \ll c/(w\alpha)$, the argument of the erf function is small (since the integration variable u is bounded by $|2\delta|$) and we can expand the erf function around 0. Note that for a collection angle of 2° , a waist $w = 30 \mu\text{m}$ and a central wavelength $\lambda = 810 \text{ nm}$, the condition of narrow filter selects wavelengths much smaller than about 100 nm , a very common configuration. Performing the expansion to the third order in δ and solving the integral, we find

$$R_{\text{tot}} \approx 128\mathcal{N}^2 \frac{\sqrt{2}\pi L^2 \tau_p \delta^2 r^2}{w^2(1+2r^2)^2} \left[1 - \frac{\alpha^2 w^2 \delta^2 r^2}{3c^2(1+2r^2)} \right]. \quad (55)$$

Hence, in presence of narrow filters, for which only the first term in the parenthesis can be considered, the brightness doesn't depend on the angle α , at least in the thin crystal limit, and its maximum is at $r^* = 1/\sqrt{2}$. Note also that the perfect phase matching approximation is well satisfied, since we are only selecting a small range of frequencies around Ω_i, Ω_s for which $\Delta k_z(\Omega_i, \Omega_s) = 0$.

C. The sinc contribution

The last missing ingredient in our thin limit discussion is the sinc contribution in (35), which we will only introduce numerically. In Figure 4 we report a plot of the optimal value of r , obtained using the thin limit bi-photon wavefunction (35) which includes the sinc contribution. The simulations have been performed for Type I SPDC, $e \rightarrow o + o$, with degenerate emission and central pump wavelength at $\lambda_0 = 405 \text{ nm}$. The pump pulse duration has been fixed at $\tau_p = 10^2 \text{ fs}$. In order to satisfy the phase matching conditions, we considered a BBO crystal and used the Sellmeier equations in [22]. For each value of α , we computed the optimal angle θ between pump and optical axis to satisfy $\Delta k_z = 0$ at the central frequencies ω_0, Ω_i and Ω_s . By doing this we assured that any variation in the emission rate is only due to geometrical factors and not to phase mismatch. The domain of integration has been chosen equal to the transmission range discussed in [22]. With respect to the perfect phase matching case of Figure 2 the introduction of the sinc produces curves with a smaller slope, without changing the extreme values.

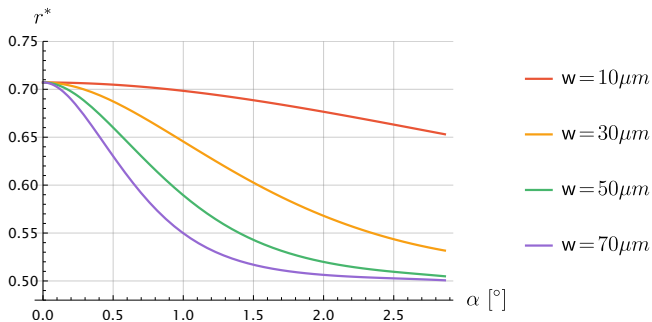


Figure 4. Optimal r to maximize the thin limit brightness including the sinc contribution, as in (35). Crystal length $L = 100 \mu\text{m}$, emission in the (x, z) plane.

V. BEYOND THE THIN CRYSTAL LIMIT

So far we discussed the brightness optimal conditions in the thin crystal limit, trying to understand the role of different experimental setups and computational assumptions. In this last section we go beyond the thin limit and report some numerical simulations obtained from the full expression of the bi-photon wavefunction, given in Equation (26). Our aim is to maximize the brightness in terms of the ratio r and the emitted photons waist w for different values of collection angle α and crystal length.

A. Setup

The simulations have been performed for degenerate Type I SPDC, $e \rightarrow o + o$, in the same setup described in Section IV C. We assumed degenerate emission in the (x, z) plane with symmetric angles of collection as in (38) and the waists configuration of (36). Simulations in the (y, z) plane do not present significant differences.

We considered two different values for the length of the crystal, $L = 100 \mu\text{m}$ and $L = 500 \mu\text{m}$, and four different values for the signal/idler waist w , from $w = 10 \mu\text{m}$ to $w = 70 \mu\text{m}$. To understand the validity of the thin crystal approximation in these cases, it is convenient to evaluate A_μ (30), which is a combination of lateral deviations and waists, and the aggregate confocal parameter ξ_μ (32). When these two quantities are very small, we can use the thin crystal approximation (34). The approximate values of A_μ and ξ_μ for our configurations are reported in Table I and II. Each quantity has been evaluated at the optimal ratio r^* .

B. Optimal ratio r

The graphs in Figure 5 represent the optimal ratios to maximize the brightness, varying the angle of collection α . Substantial deviations from the thin limit discussion emerge for all the configurations at $L = 500 \mu\text{m}$ and

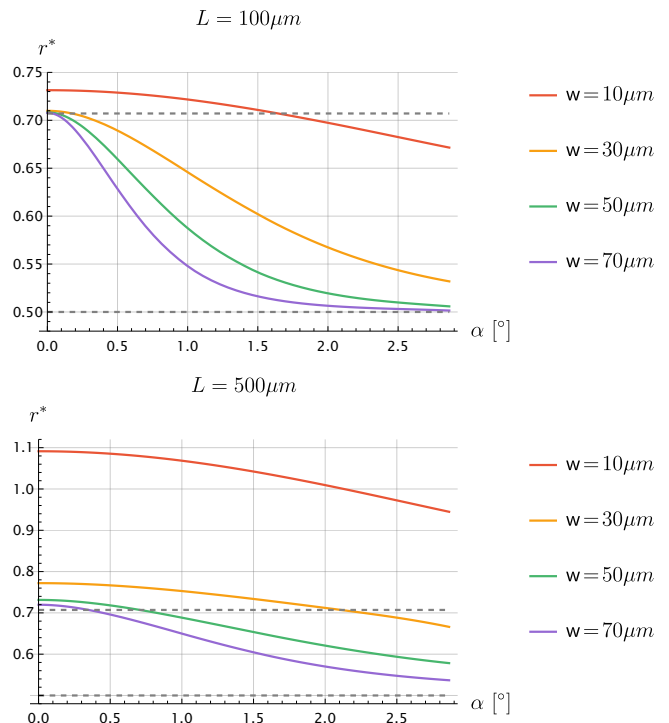


Figure 5. Transition between different optimal values moving from the collinear case to larger collection angles, at different focusing conditions. The dashed lines are at the optimal values $r^* = 1/\sqrt{2}$ and $r^* = 1/2$. Note the different scales between the two plots.

for the (rather strong) focusing condition $w = 10 \mu\text{m}$ at $L = 100 \mu\text{m}$. In all these cases, the optimal points are subjected to a shift towards larger values, compared to what found in the thin limit. At the same time, looking at the tables I and II, we note that the values of A_μ , which are related to the transverse walk-off, are significantly larger than the values of ξ_μ . It is then reasonable to suppose that the shift is mainly due to the transverse walk-off of the beams, which becomes important for longer crystals. To better justify this claim, consider the expression of the bi-photon wavefunction in Equation (26). Performing an expansion at the first order in ξ_μ ,

$L = 100 \mu\text{m}$								
w	10 μm		30 μm		50 μm		70 μm	
α	0°	2.5°	0°	2.5°	0°	2.5°	0°	2.5°
ξ_x								
ξ_y	0.07		0.008		0.003		0.001	
A_x	0	0.03	0	0.004	0	0.001	0	$7 \cdot 10^{-4}$
A_y	0.11	0.12	0.01	0.02	0.005	0.006	0.002	0.003

Table I.

we can write

$$\frac{1}{\sqrt{F_\mu}} \approx 1 - \frac{i}{2}\xi_\mu Z, \quad (56)$$

$$e^{-Z^2 \frac{Q_\mu}{F_\mu}} \approx e^{-Z^2 A_\mu} (1 + iZ^3 (B_\mu + \xi_\mu A_\mu)).$$

Assuming the longitudinal perfect phase matching approximation $L\Delta k_z \ll 1$ and substituting the expansions (56), it is easy to solve the Z -integral in (26) and find

$$\Psi(\omega_i, \omega_s) \approx 2\pi\sqrt{2}\mathcal{N}L\mathcal{A}_p^{\text{temp}}(\omega_i + \omega_s)e^{-\frac{\bar{w}^2}{2}(k_{0i\mu} + k_{0s\mu})^2} \times \frac{\text{erf}(\sqrt{A_x + A_y})}{\sqrt{A_x + A_y}} \left(\frac{\bar{w}^2}{w_p w_i w_s} \right). \quad (57)$$

Note that in this expression there is no dependence on ξ_μ , but only on the deviation parameters $\nu_{a\mu}$, which are implicit in A_μ . We now focus on the collinear emission with $\alpha = 0$. In this configuration, $A_x = 0$ while

$$A_y = \frac{L^2}{2w^2} \frac{1}{1 + 2r^2} \beta_p^2 \quad (58)$$

with

$$\beta_p = n_\theta^2 \left(\frac{1}{n_e^2} - \frac{1}{n_o^2} \right) \sin\theta \cos\theta, \quad (59)$$

where θ is the angle between the optical axis of the crystal and the propagation direction of the pump. The refraction indices in the previous expression are frequency dependent and evaluated in $\omega_p = \omega_i + \omega_s$. However, in first approximation, we can assume them to be constant and evaluate them in the fixed central frequency $\omega_p = \omega_0$. With this assumption, the collinear brightness can be derived as in (47):

$$R_{\text{tot}} \approx \frac{16\sqrt{2}\pi^{3/2}\mathcal{N}^2 d_0}{\beta_p^2 \tau_p} \frac{r^2}{(1 + 2r^2)} \text{erf} \left(\frac{L\beta_p|_{\omega_p=\omega_0}}{\sqrt{2}w(1 + 2r^2)^{1/2}} \right)^2. \quad (60)$$

The maximization of (60) with respect to r gives the orange plot in Figure 6, where instead the blue curve represents the values obtained from the full bi-photon wavefunction (26), without the expansion for small ξ_μ . For sufficiently large waists, the brightness (60) reproduces well the shifting behaviour of the optimal ratio. Since (60) depends on the deviation parameter ν_{ay} , and not on the confocal parameter ξ_μ , we can deduce that the

$L = 500 \mu\text{m}$									
w	10 μm		30 μm		50 μm		70 μm		
α	0°	2.5°	0°	2.5°	0°	2.5°	0°	2.5°	
ξ_x	0.38		0.04		0.01		0.007		
ξ_y									
A_x	0	0.86	0	0.10	0	0.03	0	0.02	
A_y	1.63	1.88	0.28	0.32	0.11	0.13	0.06	0.08	

Table II.

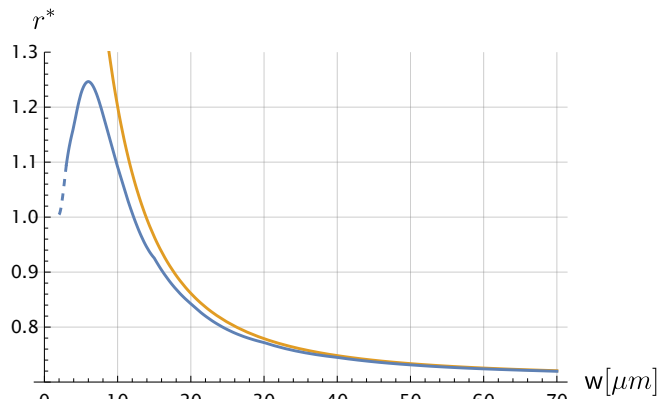


Figure 6. Optimal ratio r varying the waist w , for collinear emission, with $L = 500 \mu\text{m}$. The blue line has been obtained starting from the wavefunction (26), the orange line by maximizing (60).

shifting is mostly due to the transverse walk-off, at least in regimes far from strong focusing conditions. From a physical point of view, this result can be easily interpreted: the SPDC process can only occur if there is good overlap between the three beams in the process. The increase of the pump waist compensates for the loss of overlap due to the walk-off. Finally, we note that the importance of walk-off effects have been variously commented in the literature [7, 9, 11, 15].

1. Other SPDC processes

The above simulations and analysis were performed for Type I SPDC. Nevertheless, it is natural to expect a variation of the optimal ratio, similar to that just discussed, in all processes where transverse walk-off is present and the crystals are sufficiently long.

An important and particularly bright setup is the one in which the SPDC is realized using periodically poled crystals with collinear emission and extraordinary waves propagating along one of the principal axes. In this case there is no transverse walk-off and, in light of the previous discussion, the natural expectation for this configuration is to have $r^* = 1/\sqrt{2}$ for degenerate emission. This is in agreement with the results of [6].

C. Optimal waist w

All the expressions for the brightness derived so far have their maximum when $w \rightarrow 0$. As already discussed, however, for very small w the thin crystal limit or the expansion in ξ of the previous subsection are not justified. For this reason, we need to maximize the brightness derived from the full expression (26). Applying standard numerical method one gets the two plots in Figure 7, with

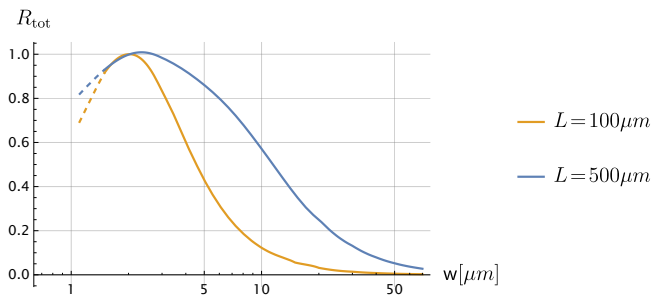


Figure 7. Normalized total brightness as function of the waist w , with $L = 500 \mu\text{m}$, in the collinear case. The curve has been produced by interpolating a finite number of waist configurations. For each waist w we first found the optimal value of r and then computed the brightness.

maxima corresponding to values of w of few micrometers. Nonetheless, the exact value of the optimal w cannot be satisfactorily obtained from our discussion: at the very beginning of our treatment we used the paraxial approximation (19), not true for extreme focusing conditions. Thus, what we can actually learn is that, at least for the lengths of the crystals considered in this work, we expect to increment the brightness by decreasing the idler/signal waist w to a value of few micrometers.

VI. CONCLUSIONS

In this work we studied degenerate SPDC emission, when the photons in the process are emitted and collected by single mode fibers. We clarified the relation between different optimal focusing conditions proposed in the literature to maximize the total brightness. In the thin crystal limit, we have given an analytical derivation of various results, considering the role of collinear and non-collinear emission, together with the finite transmission range of the crystal and the presence of spectral filters. We found that the brightness can be increased by decreasing the signal/idler waists w , assumed to be equal, whereas the optimal ratio r between the pump waist and w is $1/\sqrt{2}$ for collinear emission and tends to $1/2$ for larger angles of collection of the light. The presence of narrow spectral filters keep the optimal ratio constant to $1/\sqrt{2}$, independently on the emission angle. Moving away from the thin crystal regime, walk-off effects must be taken into account, if present, and generically the optimal ratio increases to maintain the overlap between the beams in the process: we studied this aspect in Section V where we also included numerical simulations for Type I SPDC, in a BBO crystals. To perform our numerical simulations, we used the formulas derived in Section III, which can also be used to simulate more generic SPDC processes.

Our quantitative analysis of the brightness as a function of emission angle and walk-off effects enriches discussions of other previous work, such as [6] which is

suitable for collinear emission and periodically polarized crystals. However our work is also a natural starting point for many other analyses. A first obvious generalization would be to consider non-degenerate emission or fiber collecting modes with different waists between signal and idler. Using both analytical and numerical approaches, as in this paper, it should be possible to derive the associated optimal focus conditions. Moreover it would be of great interest to extend the study to other quantities such as the heralding ratio or the spectral purity, as discussed in [6]. A careful analysis of these physical properties would lead a much deeper control of a variety of SPDC configurations and would allow the focusing conditions to be adapted to different experimental requirements.

ACKNOWLEDGMENTS

We thank Costantino Agnesi for his contribution during the initial phase of the project. Part of this work was supported by Ministero dell’Istruzione, dell’Università e della Ricerca (MIUR) under the initiative “Departments of Excellence” (Law 232/2016) and by Agenzia Spaziale Italiana (2020-19-HH.0 CUP: F92F20000000005, Italian Quantum CyberSecurity I-QKD).

Appendix A: Expansion of longitudinal component of the wavevector

In this appendix we report the expansion of the longitudinal component k_z of the wavevector around a particular value of the transverse components, inside an uniaxial crystal. We will obtain our formulas in the approximation of linear optics. We recall that we have chosen the y -axis so that the optical axis lies on the (y, z) plane. We also define θ as the angle between the optical axis of the crystal and the z -axis; n_o and n_e are the ordinary and extraordinary index of refraction.

Let us call $(x' = x, y', z')$ the frame of reference associated with the principal axes of the crystal. For an ordinary wave (i.e. polarization along the plane (x, y')) the relation between the different components of the wavevector is [23]

$$(k'_z)^2 + (k'_y)^2 + k_x^2 = n_o^2 \frac{\omega^2}{c^2}. \quad (\text{A1})$$

For an extraordinary wave, instead, the relation between k_z and the transverse components is found by solving the equation [23]

$$\frac{(k'_z)^2}{n_o^2} + \frac{(k'_y)^2 + k_x^2}{n_e^2} = \frac{\omega^2}{c^2}. \quad (\text{A2})$$

In our computation, we want to rewrite everything in terms of the basis (x, y, z) associated with the pump

beam. This can be conveniently done by using the relations

$$k'_z = \cos \theta k_z + \sin \theta k_y \quad (\text{A3})$$

$$k'_y = -\sin \theta k_z + \cos \theta k_y \quad (\text{A4})$$

which, plugged into (A1) and (A2), give equation (11).

Let's suppose now that the wavefunction is peaked around the transverse components $\bar{\mathbf{k}}_a = (\bar{k}_{ax}, \bar{k}_{ay})$, with $a = p, i, s$. In the paraxial approximation discussed in Section III, we want to expand k_{za} in powers of $\delta \mathbf{k}_a = \mathbf{k}_a - \bar{\mathbf{k}}_a$ up to the second order, namely

$$k_{az} = \bar{k}_{az} + \delta \mathbf{k}_a^\top \mathbf{K}_{1a} + \frac{1}{2} \delta \mathbf{k}_a^\top \mathbf{K}_{2a} \delta \mathbf{k}_a + \mathcal{O}(\delta \mathbf{k}_a^3). \quad (\text{A5})$$

Here $\bar{k}_{az}(\omega) \equiv k_{az}(\bar{\mathbf{k}}, \omega)$, while \mathbf{K}_{1a} and \mathbf{K}_{2a} collect the contributions of the first and the second derivatives in the expansions, having components

$$\mathbf{K}_{1a}^\mu = \left. \frac{\partial k_{az}}{\partial k_{a\mu}} \right|_{\mathbf{k}_a = \bar{\mathbf{k}}_a}, \quad \mathbf{K}_{2a}^{\mu\nu} = \left. \frac{\partial^2 k_{az}}{\partial k_{a\mu} \partial k_{a\nu}} \right|_{\mathbf{k}_a = \bar{\mathbf{k}}_a} \quad (\text{A6})$$

with $\mu = x, y$. The explicit form of \mathbf{K}_{1a} and \mathbf{K}_{2a} are given below:

$$\mathbf{K}_{1a} = \frac{1}{\beta \bar{k}_{ay} - \bar{k}_{az}} \left(\begin{array}{c} \gamma^2 \bar{k}_{ax} \\ (\beta^2 + \gamma^2 \frac{n^2}{n_o^2}) \bar{k}_{ay} - \beta \bar{k}_{az} \end{array} \right), \quad (\text{A7})$$

$$\mathbf{K}_{2a} = \frac{(\gamma n/n_o)^2}{(\beta \bar{k}_{ay} - \bar{k}_{az})^3} \left(\begin{array}{cc} (\frac{n_a \omega}{c})^2 - \gamma^2 \bar{k}_{ay}^2 & \gamma^2 \bar{k}_{ax} \bar{k}_{ay} \\ \gamma^2 \bar{k}_{ax} \bar{k}_{ay} & (\frac{n \omega}{c})^2 - \gamma^2 \bar{k}_{ax}^2 \end{array} \right) \quad (\text{A8})$$

with γ, β and n defined as in equation (11).

Appendix B: Gaussian beam in dielectric media

In this appendix we consider the Gaussian beam (15) propagating in a dielectric medium in order to clarify the physical meaning of certain quantities introduced in the main text. We call z the direction of propagation and consider the beam factorized in the x and y components so that, without loss of generality, we can focus on a generic μ -component of the field. In the momentum space we have a distribution

$$u(k_\mu) = \left(\frac{w_\mu}{\sqrt{2\pi}} \right)^{\frac{1}{2}} e^{-\frac{1}{4} w_\mu^2 (k_\mu - k_{0\mu})^2}. \quad (\text{B1})$$

The corresponding field in real space is given by

$$u(\mu, z) = \left(\frac{w_\mu}{(2\pi)^{3/2}} \right)^{\frac{1}{2}} \int dk_\mu e^{-\frac{1}{4} w_\mu^2 (k_\mu - k_{0\mu})^2 - i(\mu k_\mu + z k_z)}. \quad (\text{B2})$$

This integral expression is rather complicated due to the non trivial dependence of k_z on k_μ , as shown in (11). However, we can use a paraxial approximation, similar

to that described in Section III. The point is that the integrand in (B2) is peaked around $k_{0\mu}$, so we can expand the longitudinal component k_z as (with $\delta k_\mu = k_\mu - k_{0\mu}$):

$$u(\mu, z) = \frac{1}{\sqrt{2\pi}} \left(\frac{w_\mu}{\sqrt{2\pi}} \right)^{1/2} \times \\ \times \int dk_\mu e^{-\frac{1}{4} w_\mu^2 (k_\mu - k_{0\mu})^2} e^{-i\mu k_\mu} e^{-i(k_{0z} + \delta k_\mu K_1^\mu + \frac{1}{2} \delta k_\mu^2 K_2^{\mu\mu})z}$$

where we introduced the first and second derivative of k_z , K_1^μ and $K_2^{\mu\mu}$ respectively, evaluated on $k_{0\mu}$. The resulting Gaussian integral can be performed, obtaining

$$u(\mu, z, \omega) = \left(\frac{2}{\pi} \right)^{\frac{1}{4}} \sqrt{\frac{w_\mu}{(w_\mu^2 + 2iK_2^{\mu\mu}z)}} \times \\ \times \exp \left(-ik_{0\mu}\mu - ik_{0z}z - \frac{(\mu + K_1^\mu z)^2}{w_\mu^2 + 2iK_2^{\mu\mu}z} \right). \quad (\text{B3})$$

In this way we have found a Gaussian beam with direction of propagation described by the two wavevectors $k_{0\mu}$, k_{0z} . We stress that this interpretation holds for small values of the μ component of the wavevector, when the Gaussian profile of the absolute value of (B3) can be considered perpendicular to the propagation direction. The beam is characterized by the Siegman q -parameter in the dielectric media¹

$$q_\mu = w_\mu^2 + 2iK_2^{\mu\mu}z \quad (\text{B4})$$

and the Rayleigh range $z_{0\mu}$ is given by

$$z_{0\mu} = -\frac{w_\mu^2}{2K_2^{\mu\mu}}. \quad (\text{B5})$$

Note also that when $k_{0\mu} = 0$, (B2) differs from a Gaussian beam propagating in the vacuum along the z direction for the shifting term $-K_1^\mu z$ in the exponential. In a birefringent medium, this term could be non-zero for an extraordinary wave.

It is convenient, for a generic field, to introduce the focal parameter ($\xi_{a\mu}$) and the deviation parameter ($\nu_{a\mu}$) as in (25):

$$\xi_{a\mu}(\omega) = -\frac{L}{w_{a\mu}^2} K_{2a}^{\mu\mu}, \quad \nu_{a\mu}(\omega) = -\frac{L}{2w_{a\mu}} K_{1a}^\mu. \quad (\text{B6})$$

The parameter ξ_{ax} can also be thought as the ratio between the length L of the crystal and the Rayleigh range (B5); hence it gives information about the focusing condition of the beam in the μ direction, compared with L . The quantity $\nu_{a\mu}$, instead, parameterizes the transverse

¹ The q -parameter here defined differs from the standard q -parameter defined in [23] by a factor $-i w_\mu^2 / z_{0\mu}$, with $z_{0\mu}$ the Rayleigh range.

walk-off of the beam: as clear from (B3), at the output of the crystal, the beam is shifted by $w_{a\mu}\nu_{a\mu}$ in the μ direction. Finally note that, with these definitions, we can write the q -parameter as

$$q_{a\mu}(Z) = w_{a\mu}^2 (1 - iZ\xi_{a\mu}) , \quad (\text{B7})$$

where we also substituted $Z = 2z/L$.

Appendix C: bi-photon wavefunction in paraxial approximation

The expression (A5) gives the expansion of $k_{az}(k_{ax}, k_{ay})$ around the values \bar{k}_{ax} and \bar{k}_{ay} . To obtain an approximation of the wavefunction (8) we should also consider the expansion, around $\bar{\mathbf{k}}_i$ and $\bar{\mathbf{k}}_s$, of the phase mismatch Δk_z . Up to the second order in $\boldsymbol{\kappa}_\mu = (\delta k_{i\mu}, \delta k_{s\mu})$, we can write

$$\Delta k_z \simeq \Delta \bar{k}_z + \sum_{\mu} \boldsymbol{\kappa}_\mu \cdot \mathbf{D}_1^\mu + \frac{1}{2} \sum_{\mu\nu} \boldsymbol{\kappa}_\mu^\top \cdot \mathbf{D}_2^{\mu\nu} \cdot \boldsymbol{\kappa}_\nu \quad (\text{C1})$$

where

$$\Delta \bar{k}_z = \Delta k_z(\bar{\mathbf{k}}_s, \omega_s; \bar{\mathbf{k}}_i, \omega_i) ,$$

$$\mathbf{D}_1^\mu = \begin{pmatrix} K_{1p}^\mu - K_{1i}^\mu \\ K_{1p}^\mu - K_{1s}^\mu \end{pmatrix}, \quad \mathbf{D}_2^{\mu\nu} = \begin{pmatrix} K_{2p}^{\mu\nu} - K_{2i}^{\mu\nu} & K_{2p}^{\mu\nu} \\ K_{2p}^{\mu\nu} & K_{2p}^{\mu\nu} - K_{2s}^{\mu\nu} \end{pmatrix} .$$

Deriving the previous expression we noted that, using $k_{p\mu} = k_{i\mu} + k_{s\mu}$,

$$K_{1p}^\mu \equiv \frac{\partial k_{pz}}{\partial k_{p\mu}} = \frac{\partial k_{pz}}{\partial k_{i\mu}} = \frac{\partial k_{pz}}{\partial k_{s\mu}} \quad (\text{C2})$$

and similar relations hold for $K_{2p}^{\mu\nu}$. Then, to apply the paraxial approximation discussed in Section III, we recast the spatial mode overlap contribution

$$\mathcal{S} = u_p(\mathbf{k}_i + \mathbf{k}_s) u_s^*(\mathbf{k}_s, \omega_s) u_i^*(\mathbf{k}_i, \omega_i) \quad (\text{C3})$$

as

$$\mathcal{S} = \prod_a \left(\frac{w_{ax} w_{ay}}{2\pi} \right)^{1/2} \prod_{\mu=x,y} e^{-\frac{1}{2} \mathbf{C}_0^\mu - \boldsymbol{\kappa}_\mu^\top \cdot \mathbf{C}_1^\mu - \frac{1}{2} \boldsymbol{\kappa}_\mu^\top \cdot \mathbf{C}_2^{\mu\nu} \cdot \boldsymbol{\kappa}_\nu} \quad (\text{C4})$$

with

$$\mathbf{C}_0^\mu = \frac{1}{2} \bar{w}_\mu^2 (k_{0i\mu} + k_{0s\mu})^2 , \quad \mathbf{C}_1^\mu = 0 , \quad (\text{C5})$$

$$\mathbf{C}_2^{\mu\mu} = \frac{1}{2} \begin{pmatrix} w_{p\mu}^2 + w_{i\mu}^2 & w_{p\mu}^2 \\ w_{p\mu}^2 & w_{p\mu}^2 + w_{s\mu}^2 \end{pmatrix} \quad (\text{C6})$$

and $\mathbf{C}^{\mu\nu} = 0$ when $\mu \neq \nu$. If we now define for $j = 1, 2$

$$\mathbf{M}_j(z) = \mathbf{C}_j + iz\mathbf{D}_j \quad (\text{C7})$$

we obtain

$$\Phi(\omega_i, \omega_s) = \frac{L}{2} (2\pi)^2 \left(\prod_a \sqrt{\frac{w_{ax} w_{ay}}{2\pi}} \right) \times \int_{-1}^1 dZ e^{-\frac{iL\Delta\bar{k}_z}{2} Z} \left[\frac{e^{-\mathbf{C}_0^x - \mathbf{C}_0^y + \mathbf{M}_1(Z)^\top \mathbf{M}_2(Z)^{-1} \mathbf{M}_1(Z)}}{\det[\mathbf{M}_2(Z)]} \right]^{\frac{1}{2}} \quad (\text{C8})$$

after solving the Gaussian integral in the transverse components $\mathbf{k}_i, \mathbf{k}_s$. This result was obtained in [8], with a different choice of expansion, as explained in Section III. Introducing for each beam $a = p, i, s$ and for the x, y directions the parameters $q_{a\mu}$ and $\nu_{a\mu}$ of (B7) and (B6), the explicit form of the matrices is

$$\mathbf{M}_1 = \begin{pmatrix} \mathbf{M}_1^x \\ \mathbf{M}_1^y \end{pmatrix}, \quad \mathbf{M}_2 = \begin{pmatrix} \mathbf{M}_2^{xx} & \mathbf{M}_2^{xy} \\ \mathbf{M}_2^{xy} & \mathbf{M}_2^{yy} \end{pmatrix} \quad (\text{C9})$$

where

$$\mathbf{M}_1^\mu = iZ \begin{pmatrix} w_{i\mu}\nu_{i\mu} - w_{p\mu}\nu_{p\mu} \\ w_{s\mu}\nu_{s\mu} - w_{p\mu}\nu_{p\mu} \end{pmatrix} \quad (\text{C10})$$

and

$$\mathbf{M}_2^{\mu\nu} = i\frac{ZL}{2} \mathbf{D}_2^{\mu\nu} \quad \text{if } \mu \neq \nu , \quad (\text{C11})$$

$$\mathbf{M}_2^{\mu\mu} = \frac{1}{2} \begin{pmatrix} q_{p\mu}(Z) + q_{i\mu}^*(Z) & q_{p\mu}(Z) \\ q_{p\mu}(Z) & q_{p\mu}(Z) + q_{s\mu}^*(Z) \end{pmatrix} . \quad (\text{C12})$$

The previous expressions can be simplified by choosing particular plane of emissions, namely the (x, z) or the (y, z) planes. In these cases, the integrand in (C8) is factorized in x and y components, since this happens for the matrices \mathbf{D}_2 and \mathbf{M}_2 . The resulting expression is given in (26).

[1] V. Scarani, H. Bechmann-Pasquinucci, N. J. Cerf, M. Dusek, N. Lutkenhaus, and M. Peev, The security of practical quantum key distribution, *Rev. Mod. Phys.*

81, 1301 (2009), arXiv:0802.4155 [quant-ph].

[2] S. Pirandola, U. L. Andersen, L. Banchi, M. Berta, D. Bunandar, R. Colbeck, D. Englund, T. Gehring,

- C. Lupo, C. Ottaviani, *et al.*, Advances in quantum cryptography, *Advances in optics and photonics* **12**, 1012 (2020).
- [3] D. Bouwmeester, J.-W. Pan, K. Mattle, M. Eibl, H. Weinfurter, and A. Zeilinger, Experimental quantum teleportation, *Nature* **390**, 575 (1997).
- [4] J. L. O'Brien, Optical quantum computing, *Science* **318**, 1567 (2007).
- [5] M. A. Broome, A. Fedrizzi, S. Rahimi-Keshari, J. Dove, S. Aaronson, T. C. Ralph, and A. G. White, Photonic boson sampling in a tunable circuit, *Science* **339**, 794 (2013).
- [6] R. S. Bennink, Optimal collinear gaussian beams for spontaneous parametric down-conversion, *Phys. Rev. A* **81**, 053805 (2010).
- [7] A. Dragan, Efficient fiber coupling of down-conversion photon pairs, *Phys. Rev. A* **70**, 053814 (2004).
- [8] P. Kolenderski, W. Wasilewski, and K. Banaszek, Modeling and optimization of photon pair sources based on spontaneous parametric down-conversion, *Phys. Rev. A* **80**, 013811 (2009).
- [9] A. Ling, A. Lamas-Linares, and C. Kurtsiefer, Absolute emission rates of spontaneous parametric down-conversion into single transverse gaussian modes, *Phys. Rev. A* **77**, 043834 (2008).
- [10] R. Andrews, E. R. Pike, and S. Sarkar, Optimal coupling of entangled photons into single-mode optical fibers, *Opt. Express* **12**, 3264 (2004).
- [11] F. A. Bovino, P. Varisco, A. Maria Colla, G. Castagnoli, G. Di Giuseppe, and A. V. Sergienko, Effective fiber-coupling of entangled photons for quantum communication, *Optics Communications* **227**, 343 (2003).
- [12] G. D. Boyd and D. A. Kleinman, Parametric interaction of focused gaussian light beams, *Journal of Applied Physics* **39**, 3597 (1968), <https://doi.org/10.1063/1.1656831>.
- [13] S. Castelletto, I. Degiovanni, G. Furno, V. Schettini, A. Migdall, and M. Ware, Two-photon mode preparation and matching efficiency: definition, measurement, and optimization, *IEEE Transactions on Instrumentation and Measurement* **54**, 890 (2005).
- [14] A. Fedrizzi, T. Herbst, A. Poppe, T. Jennewein, and A. Zeilinger, A wavelength-tunable fiber-coupled source of narrowband entangled photons, *Opt. Express* **15**, 15377 (2007).
- [15] C. Kurtsiefer, M. Oberparleiter, and H. Weinfurter, High-efficiency entangled photon pair collection in type-II parametric fluorescence, *Phys. Rev. A* **64**, 023802 (2001).
- [16] D. Ljunggren and M. Tengner, Optimal focusing for maximal collection of entangled narrow-band photon pairs into single-mode fibers, *Phys. Rev. A* **72**, 062301 (2005).
- [17] J.-L. Smir, M. Deconinck, R. Frey, I. Agha, E. Diamanti, and I. Zaquine, Optimal photon-pair single-mode coupling in narrow-band spontaneous parametric downconversion with arbitrary pump profile, *J. Opt. Soc. Am. B* **30**, 288 (2013).
- [18] N. Quesada and J. E. Sipe, Why you should not use the electric field to quantize in nonlinear optics, *Opt. Lett.* **42**, 3443 (2017).
- [19] J. Schneeloch, S. H. Knarr, D. F. Bogorin, M. L. Levangie, C. C. Tison, R. Frank, G. A. Howland, M. L. Fanto, and P. M. Alsing, Introduction to the absolute brightness and number statistics in spontaneous parametric down-conversion, *Journal of Optics* **21**, 043501 (2019).
- [20] M. H. Rubin, D. N. Klyshko, Y. H. Shih, and A. V. Sergienko, Theory of two-photon entanglement in type-II optical parametric down-conversion, *Phys. Rev. A* **50**, 5122 (1994).
- [21] R. W. Boyd, *Nonlinear Optics, Third Edition*, 3rd ed. (Academic Press, Inc., USA, 2008).
- [22] D. Eimerl, L. Davis, S. Velsko, E. K. Graham, and A. Zalkin, Optical, mechanical, and thermal properties of barium borate, *Journal of Applied Physics* **62**, 1968 (1987), <https://doi.org/10.1063/1.339536>.
- [23] B. E. A. Saleh and M. C. Teich, *Fundamentals of Photonics* (Wiley, 1991).